Properties of Polypropylene/Layered-Silicate Nanocomposites and Melt-Spun Fibers

Seung Hwan Lee, Jae Ryoun Youn

Research Institute of Advanced Materials, Department of Materials Science and Engineering, Seoul National University, Shillim-Dong, Gwanak-Gu, Seoul 151-744, Korea

Received 5 November 2007; accepted 30 January 2008
DOI 10.1002/app.28222
Published online 15 April 2008 in Wiley InterScience (www.interscience.wiley.com).

ABSTRACT: Polypropylene (PP)/layered-silicate organoclay nanocomposites and their fibers were prepared by melt compounding and melt spinning, respectively, in the presence or absence of compatibilizer (PP-based maleic anhydride compatibilizer) to examine the effects of the organoclay dispersion and rheological behavior on the internal structure and tensile properties of the nanocomposite fibers. The compatibilized nanocomposites showed solidlike plateau behavior and strain hardening due to a three-dimensional network structure in the shear and uniaxial elongational flows. The tensile properties of the nanocomposite fibers were reduced compared with those of the pure PP fibers because some of the layered silicates were present as partially aggregated forms and the molecular weight of the compatibilizer was lower than that of the pure PP matrix. It was also found that the tenacity of the nanocomposite fiber increased and then decreased as the compatibilizer content increased because the compatibilizer affected the internal structure of the nanocomposite fibers. The positive effect of the compatibilizer was to generate a more effective exfoliated structure of organoclay in the polymer matrix. The negative effect was that the melt-spun nanocomposite fiber had a lower molecular weight than the pure PP fiber because the compatibilizer had a lower molecular weight. J Appl Polym Sci 109: 1221–1231, 2008

Key words: compatibilization; fibers; nanocomposites; rheology

INTRODUCTION

Reinforcing fillers are inert solid materials that are dispersed in the polymer matrix without significantly affecting the molecular structure of the polymer matrix. Recently, there has been keen interest in the development of polymer composites to improve the physical properties of polymer matrices by reinforcement with fillers. Various fillers can be used to improve the physical properties of the polymer matrix, such as mica, smectite, and montmorillonite (MMT). Among them, MMT is the one of the most common fillers because of its superior geometrical characteristics and low price. Polymer/MMT nanocomposites were first reported in the 1960s, but research activities were not carried out further until the 1990s because suitable applications were not discovered for industrial fields.[1–3]

Polymer nanocomposites are generally defined by the filler size of the dispersed phase, with at least one dimension less than 100 nm. If the dispersion at the nanoscale level is homogeneous, it leads to physical properties that cannot be attained easily from the individual components, and therefore, these nanocomposites have potential for applications as functional materials.[4] Particularly, polymer-based nanocomposites comprising organically modified layered silicates have attracted attention with the advantage that the nanoclay imposes efficient impact on the physical properties of the composites at concentrations of 5.0 wt % or less. To improve dispersion within an organic polymer, however, the sodium cation in MMT must be replaced by a different ion that is sufficiently organophilic through an ion-exchanged reaction.[5,6]

Polypropylene (PP)/layered-silicate nanocomposite is one attractive system that can lead to new materials for engineering applications and widen the versatility of PP-based materials. The homogeneous and fully exfoliated dispersion of the silicate layers could be achieved in such matrix resins as polymers with polar functional groups. However, there has been a limitation on the polymer matrix used for layered-silicate reinforced nanocomposites, such as nonpolar polymer resins. This is mostly due to the fact that the silicate layers of the organoclay have polar hydroxy groups and are compatible with polymers containing the functional groups. On the other hand, poor adhesion between the filler surface and the polymer matrix prohibits the wet-out of the silicate layers needed to help break up aggregates of particles, which results in poor dispersion,

Correspondence to: J. R. Youn (jaeryoun@snu.ac.kr).
Contract grant sponsor: Korea Science and Engineering Foundation through the Applied Rheology Center.

Journal of Applied Polymer Science, Vol. 109, 1221–1231 (2008)

insufficient reinforcement, and poor mechanical properties. To overcome these problems, one method is to make the filler surface more hydrophilic through surface treatment. Another approach is to modify the chemistry of the PP matrix by the attachment of polar groups, such as maleic anhydride based polymers.[7]

Rheological measurement is one important method for the characterization of materials because the internal structure and processability of polymeric materials can be estimated by the rheological properties. An accurate understanding of the flow behavior is decisive in the optimization of processing conditions, such as spinning temperature and speed, in fiber spinning for polymers and polymer composites.[1,8–10] For example, it is preferred for a stable fiber spinning process that the elongational viscosity should increase with the elongational rate because an increased elongational viscosity resists further stretching in the thin area. It is important to evaluate the rheological behavior in both the shear and elongational flows to understand the internal structure and processing properties of polymers and polymer composites.[11]

New fiber technologies have been developed in past years to enhance the physical properties and spinnability of polymers by the incorporation of reinforcing fillers into polymer materials.[12] However, most micrometer-scaled fillers are unsuitable for fiber spinning because they can easily lead to spinline failures because of their size, which approaches the order of the fiber diameter. Because of reduced thickness and the extremely large aspect ratio of the nanoclay, the interaction between the reinforcing nanofiller and the polymer matrix is maximized by the increase in contact area. Consequently, the nanofiller loading could be reduced to 1.0–5.0 wt % compared with conventional composites containing a high loading of reinforcing fillers. Mlynarcikova et al.[13] investigated the fiber characteristics of nanocomposites prepared by the mixture of syndiotactic PP and organoclay with octadecylammonium chains and reported that a high draw ratio of the nanocomposite fiber was achieved only through the use of the compatibilizer.

In this study, PP/layered-silicate nanocomposites were prepared with maleinated PP, and their morphological properties were investigated by small-angle X-ray scattering (SAXS) and transmission electron microscopy (TEM). The rheological behavior in the dynamic oscillatory shear and uniaxial elongational flows was investigated to evaluate the spinnability of the nanocomposite melts and to estimate the effect of the organoclay and compatibilizer loadings on the dispersion and interfacial interaction of the layered-silicate organoclay (OLS). Then, fiber spinning was performed to investigate the effects of the spinning conditions on the internal molecular structure and tensile properties of the nanocomposite fibers. Finally, their fiber characteristics were discussed through the analysis of the interrelations among the spinning conditions, organoclay and compatibilizer contents, and structural parameters, such as the degree of exfoliation and crystallinity in the nanocomposite fibers.

TABLE I
Molecular Weight and MFR Values of the PP Matrix and PP-*g*-MAH Compatibilizer

	MFR	M_n	M_w	M_w/M_n
MOPLENE HP552N	12.0	60,318	343,632	6.25
PP-*g*-MAH	50.0	56,157	295,559	7.75

The MFR of the pure PP matrix and PP-*g*-MAH compatibilizer was measured at 230°C and 2.16 kg. M_n = number-average molecular weight; M_w = weight-average molecular weight.

EXPERIMENTAL

Materials

We prepared the PP/layered-silicate nanocomposites by combining isotactic polypropylene resin (iPP), OLS, and polypropylene-based maleic anhydride compatibilizer (PP-*g*-MAH). An iPP matrix manufactured for fiber spinning was supplied by Polymirae (MOPLENE HP552N, Seoul, Korea). It had a melt flow rate (MFR) of 12.0 g/10 min and a melting point of 162°C. Na^+-based MMT with a cation-exchange capacity value of 125 mmol/100 g and OLS were supplied by Southern Clay Products (Cloisite 15A, Gonzales, TX). The compatibilizer, supplied by Crompton (Polybond 3150, Middlebury, CN), was added to promote the interaction due to hydrogen bonding between the PP matrix and organoclay layers. Its MFR was 50 g/10 min, and its grafted maleic anhydride content was 0.5 wt %. The molecular properties of the pure PP matrix and PP-*g*-MAH compatibilizer used in this study are listed in Table I.

Melt compounding and fiber spinning

All samples were prepared by melt compounding at 210°C and at a screw speed of 350 rpm with a twin-screw extruder (ZSK-25 type, Werner & Pfleiderer, Tamm, Germany). The compounded melt was extruded, and the extrudate was quenched in water and pelletized. Specimens of the nanocomposites containing PP matrix, PP-*g*-MAH compatibilizer, and OLS were produced, and their compositions are illustrated in Table II. Pure PP and melt-compounded nanocomposite pellets were dried in a vacuum oven for 4 h at 80°C before melt spinning. Melt

TABLE II
Compositions (wt %) of the Prepared Nanocomposites Based on PP, PP-*g*-MAH, and Organoclay

Sample	Pure PP (HP552N)	PP-*g*-MAH (Polybond 3150)	Organoclay (Cloisite 15A)
iPP[a]	100		
iPP/05	95	5	
iPP/00/OLS0.5	99.5		0.5
iPP/00/OLS01	99		1
iPP/00/OLS02	98		2
iPP/00/OLS03[b]	97		3
iPP/00/OLS05	95		5
iPP/05/OLS0.5	94.5	5	0.5
iPP/05/OLS01	94	5	1
iPP/05/OLS02	93	5	2
iPP/05/OLS03[c]	92	5	3
iPP/05/OLS05	90	5	5
iPP/01/OLS03	96	1	3
iPP/03/OLS03	94	3	3
iPP/07/OLS03	90	7	3

[a] Pure PP: MFR = 12.0 g/10 min.
[b] iPP/00/OLS03: uncompatibilized nanocomposite.
[c] iPP/05/OLS03: PP-*g*-MAH compatibilized nanocomposite.

spinning was performed on a single-screw extruder (length/diameter = 30, Polymirae) with a spinneret containing 60 holes, each hole with a diameter of 0.5 mm and a length of 1.0 mm. The extruder was set with four different temperature zones of 190, 210, 230, and 240°C at feeding, metering, melting, and spinneret sections, respectively. The as-spun filaments were collected at a take-up speed of 500–1250 m/min and a draw ratio of 1.0 at room temperature. The spinning conditions used in this study are presented in Table III.

Characterization

A Rigaku Max-3 Cg X-ray diffractometer (Tokyo, Japan) with Cu Kα radiation (λ = 0.154184 nm) was used to determine the interlayer spacing of the organoclays for the PP/layered-silicate nanocomposites. The wide-angle X-ray diffraction (WAXD) patterns of the PP and nanocomposite fibers were obtained by an X-ray diffractometer (Bruker AUX D8 Advance with general area detector diffraction system (GADDS), 40 kV, 40 mA, Cu Kα, Germany) in a scanning range of 2θ = 0–40°, where 2θ is the diffraction angle. A transmission electron microscope (JEM-2000EXII, 200 kV, Tokyo, Japan) was used to observe the dispersion state of organoclays in the nanocomposites. TEM specimens were microtomed to an ultrathin section with a thickness of about 100 nm and coated with carbon for 5 min to prevent specimens from degrading by the irradiation of electrons.

TABLE III
Spinneret Geometries and Spinning Conditions Used for the PP and Nanocomposite Fibers

Parameter	Processing conditions
Temperature (°C)	240
Spinning speed (m/min)	500, 750, 1000, 1250
Draw ratio	1
Amount of organoclay (wt %)	0, 0.5, 1.0, 2.0, 3.0, 5.0
Amount of compatibilizer (wt %)	0, 1.0, 3.0, 5.0, 7.0

The spinning materials were iPP, iPP/00/OLS03, and iPP/05/OLS03. The spinneret dimensions were as follows: 60 holes × 0.5 mm diameter × 1.0 mm length.

We measured the MFR values of various samples by weighing the run under 2.16 kg at 230°C using a melt flow indexer (Melt Indexer MI-3, Göttfert, Dresden, Germany) to verify the possibility of the melt spinning of the nanocomposite melts. Dynamic oscillatory shear flow measurements were conducted with a rotational rheometer (AR-2000, TA Instruments, New Castle, DE) with parallel plates. Frequencies of 0.01–200 rad/s were used at a strain amplitude of 10% to be within the linear viscoelastic region. The viscosity growth during the uniaxial elongational flow at a constant elongation rate was measured with a Meissner-type rheometer (Rheometrics elongational rheometer (RME), Rheometric Scientific, Piscataway, NJ). Constant elongation rates were applied at elongation rates of 0.05, 0.1, 0.3, 0.5, and 1.0 s^{-1}.

The linear fiber density was determined at ambient temperature with a yarn measuring system (Zweigle L232, Zweigle Textilprüfmaschinen, Reutlingen, Germany). The tensile strength and elongation at break of the pure PP and nanocomposite fibers were measured at ambient temperature with a textile tensile tester (Uster Tensorapid-4, Zellweger Uster, Switzerland). The gauge length was 200 mm, and the deformation rate was 100 mm/min for as-spun fibers. The tensile strength and elongation at break of fibers were calculated from the stress–strain curve. The tensile strength was determined from the top of the stress–strain curve, and the elongation at break was determined from the distance between the start and the point of break. All tensile properties are reported in terms of an average of 10 samples.

RESULTS AND DISCUSSION

Morphology and rheological properties of the nanocomposites

The SAXS spectra patterns for the organoclay powders, the pure PP matrix, the uncompatibilized composites, and two types of compatibilized nanocomposites are shown in Figure 1. The SAXS spectra of the original organoclay powder showed the peak of

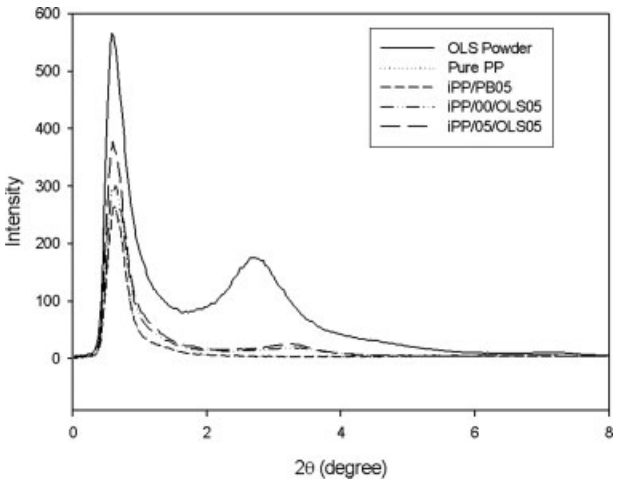

Figure 1 SAXS patterns of the organoclay powder, pure PP, uncompatibilized nanocomposite (iPP/00/OLS05), and compatibilized nanocomposite (iPP/05/OLS05).

intensity at 2θ = 2.65°, and the equivalent distance between silicate layers was 34.46 Å. The SAXS pattern of the compatibilized nanocomposites did not show the characteristic basal peak of the organoclay. This indicated that the strong interaction between polar groups of the compatibilizer and functional groups of the silicate layers had been formed and PP chains had intercalated into the gallery of organoclay. However, the SAXS spectra patterns of the organoclay-filled nanocomposites displayed a slight increase in the intensity at lower 2θ values when compared to that of the unfilled PP matrix. However, as shown in Figure 1 and Table IV, both the uncompatibilized and compatibilized nanocomposite systems with organoclay showed weak (002) plane peaks at about 2θ = 3.32°. Although most of the organoclay was fully exfoliated, it is feasible that thermal degradation occurred at some of the ion-exchanged organoclay during melt compounding and that there was insufficient shear stress to exfoliate the organoclay during melt compounding because of low molecular weight of the PP matrix (MFR = 12.0 g/10 min).[14,15]

Although X-ray scattering is useful for the measurement of the space distance between intercalated layered silicates in nanocomposites, it may be insufficient for the measurement of disordered and exfoliated materials that do not give any peak. Therefore, further investigation of the organoclay dispersion in the PP matrix was performed by TEM observation and rheological measurement in the shear and elongational flows. First, TEM images for the uncompatibilized and compatibilized nanocomposites were observed to identify the dispersion state of the silicate layers and are shown in Figures 2 and 3. In the case of the uncompatibilized composites, the silicate layers were aggregated with a size of several hundreds of nanometers, as shown in Figure 2(a,b).

TABLE IV
2θ and *d*-Spacing Values Measured from the SAXS Patterns for the Organoclay Powder, Uncompatibilized Nanocomposite (iPP/00/OLS03), and PP-*g*-MAH Compatibilized Nanocomposite (iPP/05/OLS03)

	2θ (°)		*d*-spacing	
Sample	(001)	(002)	(001)	(002)
Cloisite 15A	2.68	—	3.45	—
iPP/00/OLS05	—	3.33	—	2.74
iPP/05/OLS05	—	3.20	—	2.68

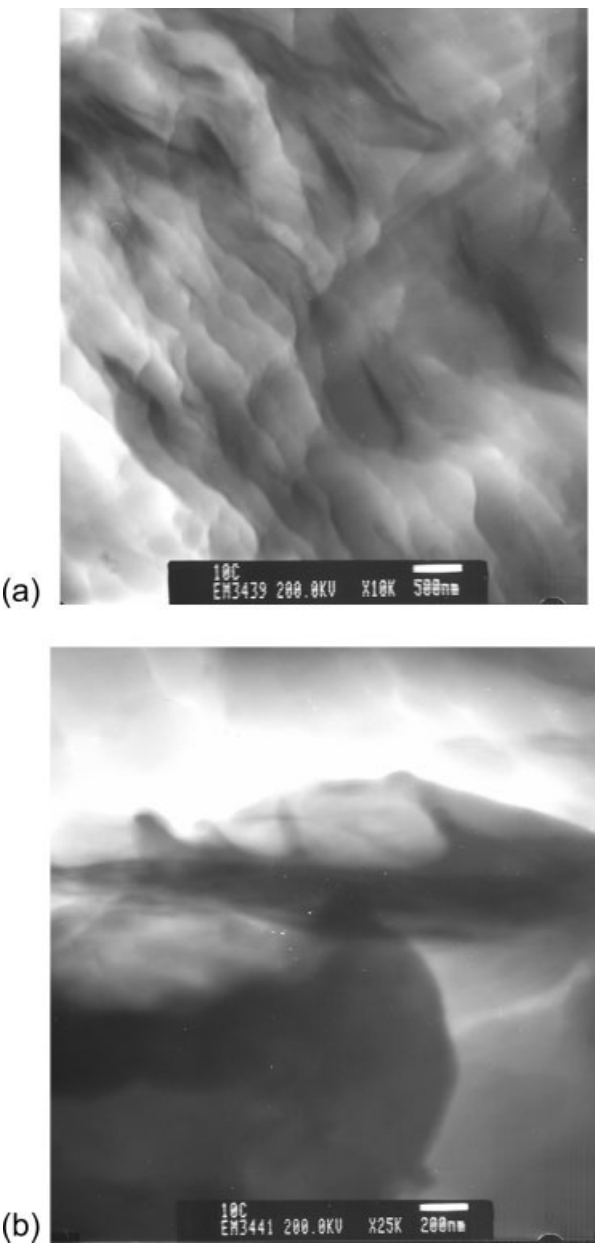

Figure 2 TEM images of (a) low (10,000×) and (b) high (25,000×) magnification for the uncompatibilized nanocomposites (iPP/00/OLS05).

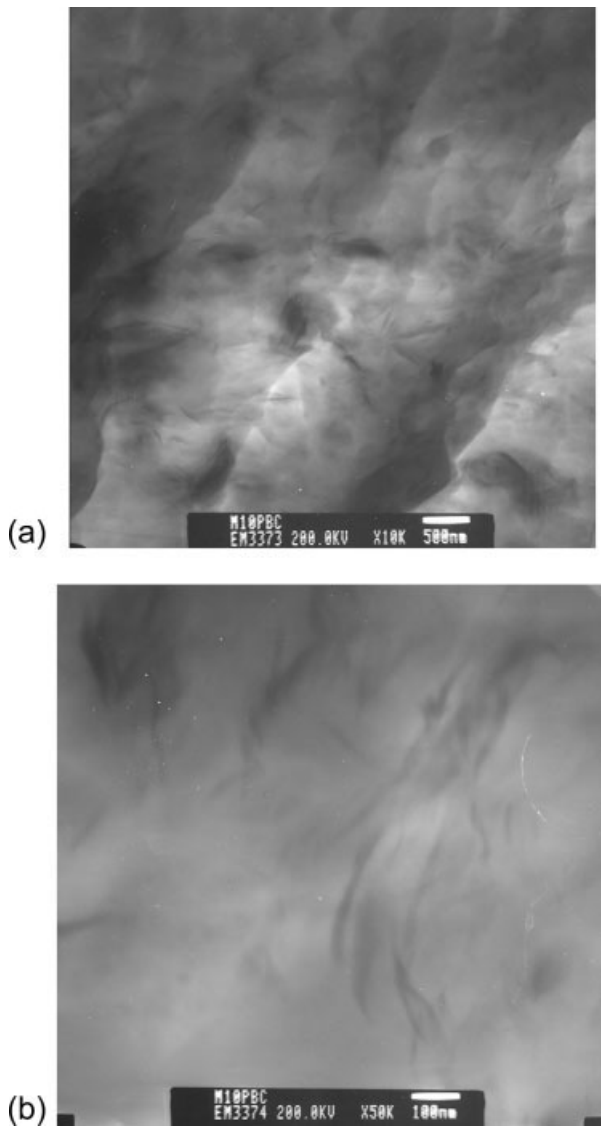

Figure 3 TEM images of (a) low (10,000×) and (b) high (50,000×) magnification for the compatibilized nanocomposites (iPP/05/OLS05).

However, the micrograph of the PP-*g*-MAH compatibilized nanocomposite showed that individual exfoliated platelets were embedded in the PP matrix, as shown in Figure 3. Each layer of the organoclay was dispersed homogeneously in the PP matrix, although a small amount of intercalated layers still existed. From the previous experimental results on the internal structure of the nanocomposites, it was apparent that the PP-*g*-MAH compatibilizer improved the dispersity and homogeneity of the layered silicates in the PP matrix.[16–18]

Characteristic rheological properties of the nanocomposites were investigated to examine the internal structure with respect to the nanoscale dispersion of the organoclay particles. First, MFR was investigated to verify the spinning possibility of the PP/layered-silicate nanocomposite melts. Table V shows the influence of the organoclay and compatibilizer loadings for each nanocomposite on the MFR. Although the MFR of the iPP/05 blend was higher than that of the pure PP matrix, it became slightly lower than that of the pure PP matrix when an organoclay loading of 3.0 wt % was added without the compatibilizer. ''iPP/05'' is the blend sample prepared with polypropylene matrix and PP-*g*-MAH of 5.0 wt % without organoclay, as shown in Table V. The number ''05'' represents the weight fraction of PP-*g*-MAH compatibilizer. The MFRs of the compatibilized nanocomposites with the same organoclay loading of 3.0 wt % decreased slightly from 11.56 to 10.55 as the loading of compatibilizer increased from 1.0 to 7.0 wt % because molecular interaction among the PP matrix, functional groups of organoclay, and maleic anhydride groups of the compatibilizer increased. However, we confirmed that the MFR of the melt-compounded PP/layered-silicate nanocomposite melt was large enough for melt spinning with a conventional spinning machine.

The rheological properties of various PP/layered-silicate nanocomposites were investigated by rotational and extensional rheometers in both shear and elongational flows. In Figure 4(a,b), the storage modulus and complex viscosity are compared to identify the difference in shear flow properties between the two kinds of nanocomposite. The pure PP matrix showed classical viscoelastic behavior, a terminal flow regime where the storage modulus was proportional to ω^2, where ω is the angular frequency. The uncompatibilized nanocomposite [iPP/00/OLS05 (05 is the weight fraction of OLS [organically modified layered silicate])] showed a small deviation from classical behavior at lower frequencies. There was a slight increase in the storage modulus with increasing clay content, and only a weak solidlike plateau behavior was observed in the low-frequency region. However, in the case of the PP-*g*-MAH compatibilized nanocomposite (iPP/05/OLS05) melts, the storage modulus showed nonterminal plateau solidlike behavior and had a higher value than that of the

TABLE V
Influence of the Organoclay and Compatibilizer Contents on the MFR for Each Nanocomposite System

Sample	Pure PP (HP552N)	PP-*g*-MAH (Polybond 3150)	Organoclay (Cloisite 15A)	MFR
iPP	100			12.35
iPP/05	95	5		13.95
iPP/00/OLS03	97		3	11.32
iPP/05/OLS03	92	5	3	10.64
iPP/01/OLS03	96	1	3	11.56
iPP/03/OLS03	94	3	3	11.02
iPP/07/OLS03	90	7	3	10.55

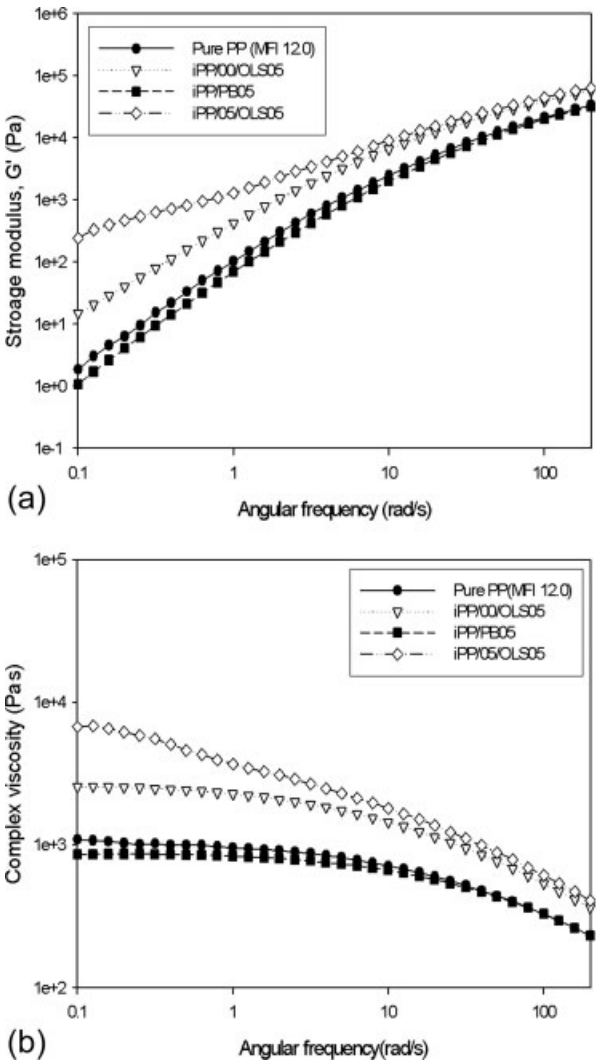

Figure 4 Frequency dependence of the (a) storage modulus and (b) complex viscosity for the pure PP, uncompatibilized nanocomposite, and PP-*g*-MAH compatibilized nanocomposites.

pure PP matrix or uncompatibilized nanocomposites at low-frequency ranges.[8,10,19]

The solidlike plateau behavior became distinct as the organoclay content increased. As the amount of well-dispersed clay increased, a network structure was formed because of the close interaction between the clay particles and hydrodynamic interaction between the clay particles and polymer chains. Kotsilkova, Ren, and coworkers[20,21] also reported that the organoclay produced a larger shift in the relaxation spectrum toward longer relaxation timescales than that of the pure polymer matrix because the two-phase structure of poly(methyl methacrylate)/smectite clay nanocomposites caused retardation of the complete polymer relaxation. The domain structure of the silicate layers oriented in some preferable direction, and the lack of complete relaxation of the molecular chains contributed to the solidlike behavior of the polymer nanocomposites at low frequencies.

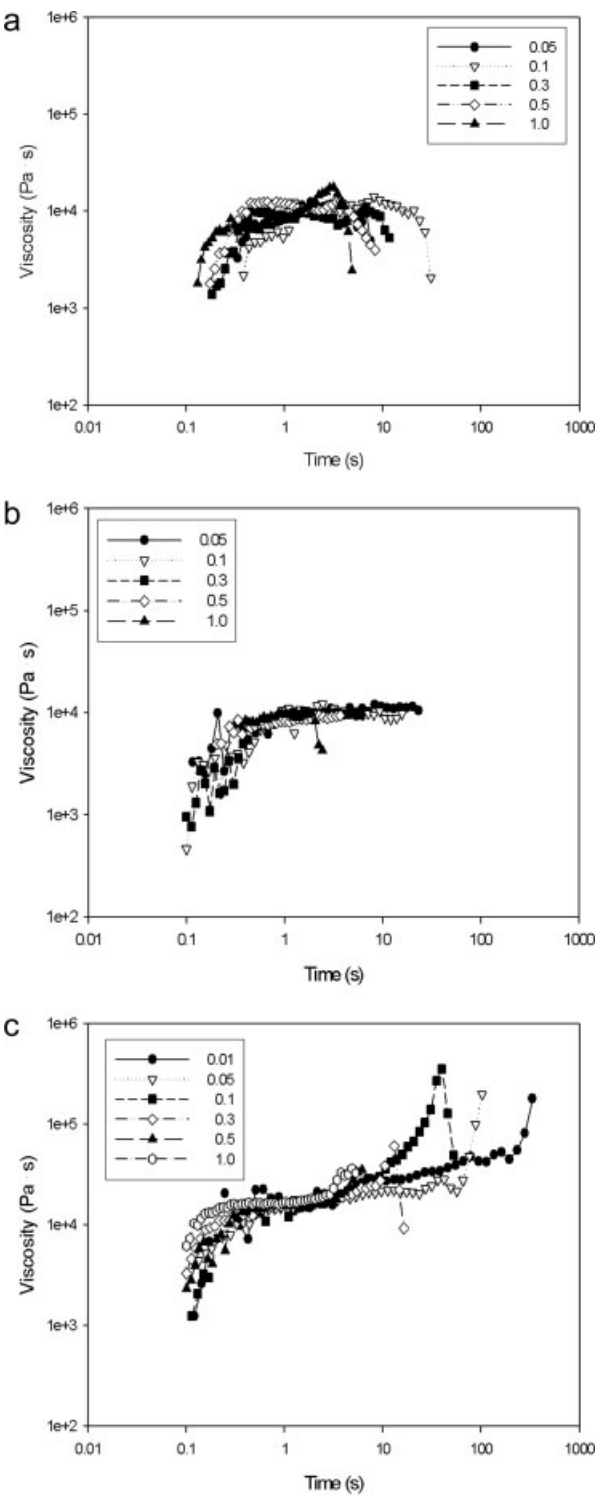

Figure 5 Elongational viscosity growth curves of the (a) pure PP, (b) uncompatibilized composite (iPP/00/OLS05), and (c) PP-*g*-MAH compatibilized nanocomposite (iPP/05/OLS05) melts at different elongational strain rates (temperature = 190°C).

Figure 5 shows the elongational viscosity observed for the pure PP, uncompatibilized nanocomposites, and PP-*g*-MAH compatibilized nanocomposites with different elongational rates ranging from 0.01 to 1.0 s^{-1}. In the case of the pure PP matrix and uncompatibilized composites, the elongational viscosity increased linearly with time, and strain hardening was not observed. In the case of the PP-*g*-MAH compatibilized nanocomposites, the initial parts of all of the elongational viscosity growth curves showed simple monotonic growth that agreed well with the theory of linear viscoelasticity. After extensional deformation equivalent to the Hencky strain ($\varepsilon = \dot{\varepsilon} \times t$; where $\dot{\varepsilon}$ is the elongational strain rate and t is time) of about 1.0, some of the growth curves showed strong strain hardening as the elongation rate increased. Like the solidlike behavior shown in dynamic oscillatory shear flow, the strain hardening of the compatibilized nanocomposite was generated by the three-dimensional network structure formed by strong molecular interaction between the PP chains and layered silicates with the aid of the compatibilizer. Consequently, we expected that the spinnability of the compatibilized nanocomposites may have been improved at higher elongational rates during fiber spinning. Takahashi et al.[22,23] reported many research results on the strain hardening of polymer blends or composites in elongational flow and demonstrated that strain hardening was enhanced by the existence of a long relaxation time, which came from a wide molecular weight distribution and a long-chain branched structure with increased chain entanglements.

Internal structure and tensile properties of the nanocomposite fibers

PP fibers are produced commercially in various types with different tenacities to satisfy various market requirements. The tenacity of PP fibers is in the range 4.0–6.0 g/den for general purpose textiles. High-tenacity fibers of up to 8.0 g/den are produced for industrial applications, such as ropes and nets.[24] There are two structural parameters that affect the physical properties of nanocomposite fibers, that is, the extent of exfoliation and the degree of crystallinity. They are also important because the tensile properties depend on the internal structure of the fiber, and they are sensitive to spinning conditions. In general, the nanometer-scale organoclay layers dispersed in the polymer matrix act as heterogeneous nucleation sites for crystallization and augment the nucleation rate, which leads to an increase in the crystallization rate of the as-spun nanocomposite fibers.[25] Meanwhile, the crystallinity of the nanocomposite fibers was much higher than that of the pure PP fibers produced under the same spinning conditions, whereas the molecular orientation of the nanocomposite fibers was much lower than that of the pure PP fibers. Therefore, two types of nanocomposite fibers were prepared in this study to investigate the correlations among the tensile properties, crystallinity, and exfoliation structure.

The tensile strength and elongation at break of the pure PP and nanocomposite fibers are plotted with respect to take-up speed in Figure 6(a,b). The tensile strength of the pure PP fibers increased as the take-up speed was raised up to 1000 m/min and slightly decreased thereafter. Although the tensile strength of the nanocomposite fibers was lower than that of the pure PP fibers, those of both the uncompatibilized and compatibilized nanocomposite fibers increased in the experimental take-up speed ranges, and the extent of the increase for the compatibilized nano-

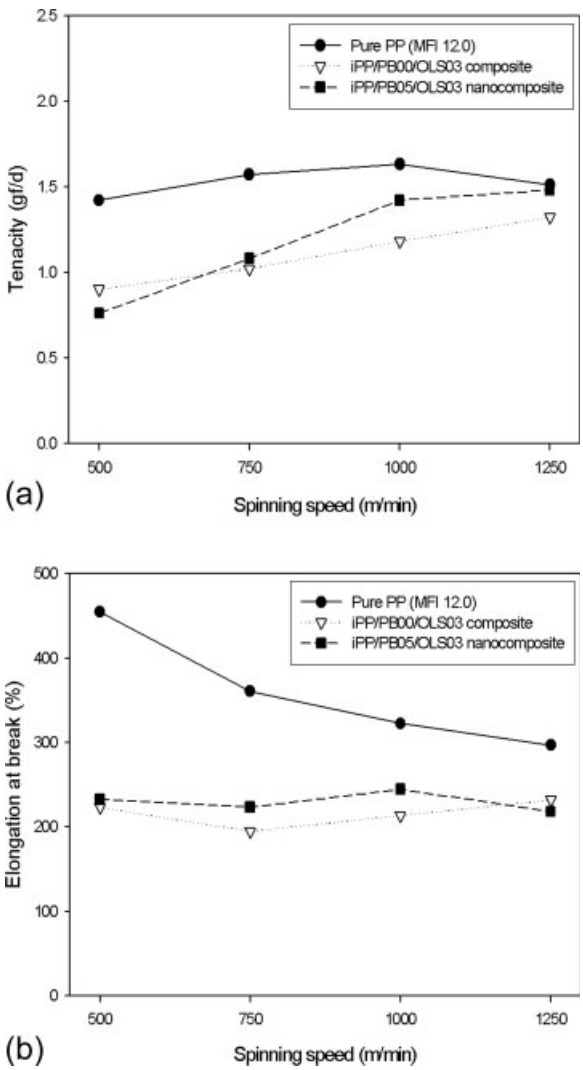

Figure 6 Effects of spinning speed on the (a) tensile strength and (b) elongation at break of the pure PP, uncompatibilized nanocomposite, and compatibilized nanocomposite fibers.

composite fibers was bigger than that of the uncompatibilized nanocomposite fiber. In addition, the elongation at break of the pure PP fibers gradually decreased in the experimental ranges because of a slightly increased molecular orientation. In the case of both nanocomposite fibers, however, the elongation at break remained constant regardless of the take-up speed because some layered silicates were still present as partially aggregated forms, as shown in the SAXS patterns. It is well known that nanometer-scale dispersions of silicate layers in the polymer matrix lead to improved tensile properties. Particularly, the silicate layers contribute to the presence of immobilized or partially immobilized polymer chains and provoke enhanced tensile properties of the nanocomposite fibers. To improve the tensile properties of the nanocomposite fibers, it is necessary to produce the fibers at low organoclay loadings for the orientation of both silicate layers and molecular chains during fiber spinning. From the previously discussed results, we confirmed that the PP-*g*-MAH compatibilizer used in this study gave a more exfoliated structure at higher take-up speed despite a higher organoclay loading of 3.0 wt %.

The effects of the organoclay and compatibilizer on the exfoliation structure and crystalline morphology of the nanocomposite fibers were characterized in connection with their tensile properties. In Figure 7(a,b), the WAXD patterns illustrate how take-up speed affected the crystal formation and the extent of exfoliation of the as-spun nanocomposite fibers when the organoclay and compatibilizer were added and different take-up speeds of 500 and 1250 m/min were applied. There was little difference in the exfoliated and crystalline structure between two types of melt-spun nanocomposite fibers produced at the take-up speed of 500 m/min, as shown in Figure 7(a). However, we found that a more exfoliated structure was formed in the PP-*g*-MAH compatibilized nanocomposite fibers as the take-up speed was increased up to 1250 m/min, as shown in the peak intensity of small-angle ranges [0–10°; Fig. 7(b)].

The WAXD results indicate that the crystal type of the nanocomposite fibers did not change and was still in the α-monoclinic crystal form, as shown in the peak intensity of wide-angle ranges. Although we also found that the PP and nanocomposite fibers exhibited different crystalline diffraction peak intensities, the peak position of every crystal plane did not shift just because organoclay and compatibilizer were added. An important observation from Figure 7 is that relative to the intensity of the (110) plane peak, the intensities of the other α-phase peaks, that is, (040), (130), and (111) planes, increased with the addition of organoclay. Zheng et al.[26] investigated the crystalline morphology and crystallization rate of PP/organoclay nanocomposites using various thermomechanical methods. According to their report, pure PP and as-extruded PP/organoclay nanocomposites contained only α-phase crystallites because of the rapid cooling of the melts. Although β-phase crystallites can be formed in pure PP under various thermal conditions, β-phase crystallites were not generated in the PP/organoclay nanocomposites because the organoclay inhibited the formation of β-form crystallites. The organoclay in the PP matrix accelerated the crystallization process of the α-phase crystallites but had no effect on the crystallization of the β-phase crystallites. Therefore, the nucleation rate of the PP crystals in the nanocomposite fibers prepared in this study was promoted by the addition of organoclay, and perfect α-phase crystallites were generated.

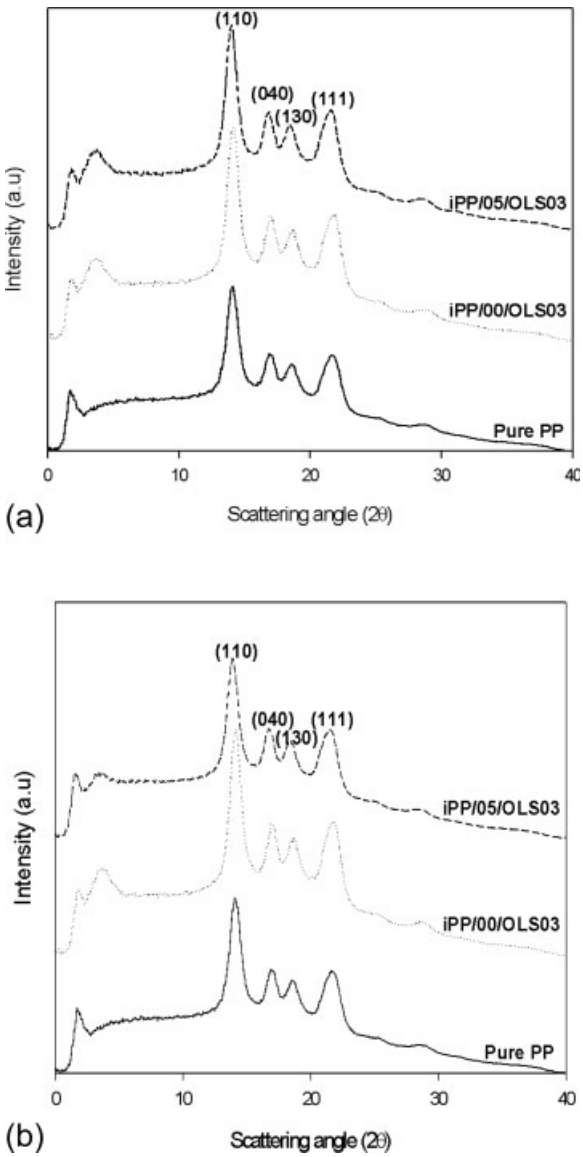

Figure 7 WAXD patterns for PP and two types of nanocomposite fibers produced at different spinning speeds of (a) 500 and (b) 1250 m/min.

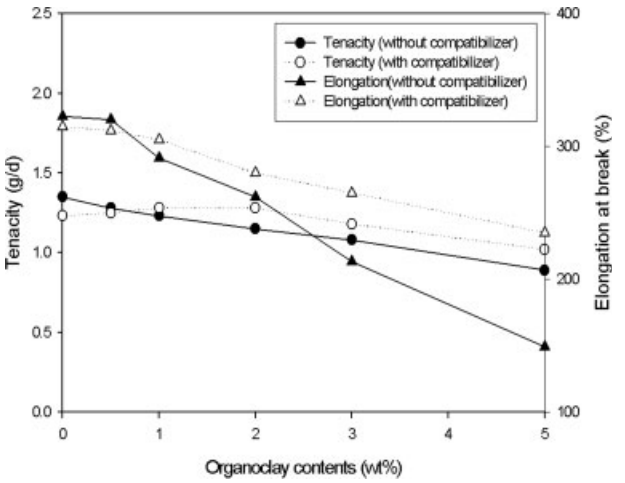

Figure 8 Effects of the organoclay loadings on the tensile properties of the uncompatibilized nanocomposite fibers and compatibilized nanocomposite fibers with 5.0 wt % PP-*g*-MAH compatibilizer.

The tensile properties of the nanocomposite fibers were also investigated to evaluate the reinforcing effect of the organoclay and the PP-*g*-MAH compatibilizer at the same spinning conditions. Figure 8 shows effects of the organoclay loadings on the tensile properties of the nanocomposite fibers with or without the compatibilizer. The tenacity and elongation at break of both uncompatibilized and compatibilized nanocomposite fibers remained at the same level as those of the pure PP fibers for organoclay concentrations of up to 2.0 wt % and then decreased abruptly with increasing organoclay content. At weight fractions of less than 1.0% organoclay, the compatibilized nanocomposite fibers had similar tensile strengths compared to the uncompatibilized nanocomposite fibers. Joshi and Viswanathan[27] also demonstrated that the tensile properties of PP/nanoclay composite fibers improved significantly compared with those of pure PP fibers at very low organoclay loadings, that is, 0.25–0.5 wt %, with a compatibilizer/organoclay ratio of 2 : 1 and, thereafter, tended to stabilize or decrease at higher organoclay loadings because the aggregation of the silicate layers was generated in the PP matrix. Low contents of organoclay result in dispersed domains of small sizes and uniform distributions, whereas high loadings result in large-size domains and broad domain distributions. In this study, the tensile strengths of both nanocomposite fibers were not improved compared with that of the pure PP fibers. However, the extent of the decrease in tensile strength of the compatibilized nanocomposite fibers was less than that of the uncompatibilized composite fibers.[28–30] In the case of the nanocomposite fibers with organoclay, there were small intercalated aggregates and well-dispersed domains whose size and distribution were correlated with the content of organoclay. We confirmed that a homogeneous and exfoliated dispersion of organoclay brought better properties to the final fibers.

In Figure 9, the WAXD study illustrates that the addition of organoclay and compatibilizer affected the crystal formation and extent of exfoliation of the as-spun nanocomposite fibers. We found the PP fibers and the nanocomposite fibers exhibited different crystalline diffraction peak intensities. In general, it is expected that a larger initial layer spacing will lead to easier exfoliation because platelet–platelet attraction will be reduced. It is implied that the diffusion of polymer chains into organoclay galleries is less hindered because of increased spacing and ultimately leads to improved exfoliation. The intensity of the (040) peak was much higher than that of the (111) peak at the organoclay loading of 2.0 wt %.

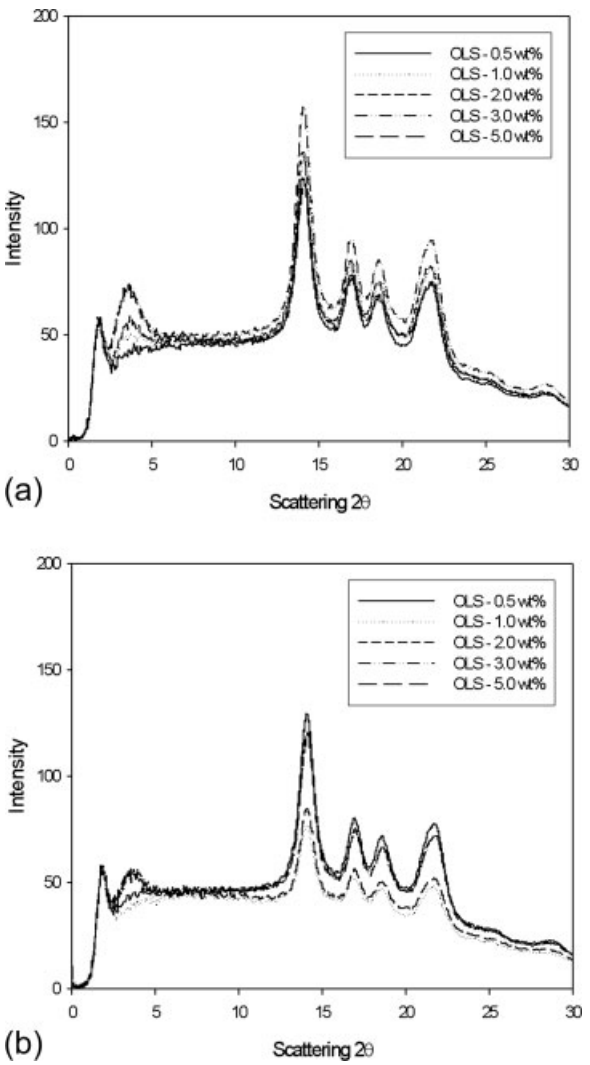

Figure 9 Effects of the organoclay loadings on the WAXD patterns of the (a) uncompatibilized nanocomposite fibers and (b) compatibilized nanocomposite fibers with 5 wt % PP-*g*-MAH compatibilizer.

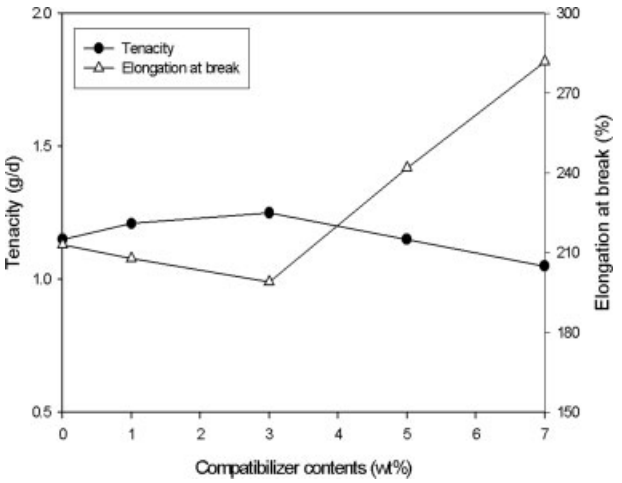

Figure 10 Effects of the PP-*g*-MAH compatibilizer on the tensile properties of the compatibilized nanocomposite fibers containing 3.0 wt % organoclay.

This fact implied that the surface of the organoclay platelets may have induced preferred orientation of the α-phase crystallites.[31–33] At lower organoclay contents, the organoclay was well exfoliated so that the organoclay platelets could be easily oriented during fiber spinning because of their large aspect ratio. The orientation of organoclay may have led to the orientation of the crystallites if crystallization was initialized on the organoclay surface in a certain flow direction. However, when the organoclay loading was larger than 3.0 wt %, the organoclay orientation was more difficult because the interaction between the organoclay particles was increased and the aspect ratio of the organoclay was reduced by the aggregates, which would have led to a more isotropic arrangement of crystallites.[34,35] The size of the crystallites that were perpendicular to the (040) crystal plane in the nanocomposite fibers was smaller than that in the pure PP fibers. It was clear that crystallite size of the nanocomposite fibers was decreased by the introduction of the compatibilizer and organoclay. Because the organoclay acted as a heterogeneous nucleating agent for the crystallization of PP and the maleic anhydride group included in the PP-*g*-MAH exhibited strong polarity, PP-*g*-MAH and OLS were inclined to absorb macromolecular segments, and consequently, chain movement was constrained to initiate crystallization. The crystal nucleation was accelerated and resulted in the increase in the overall crystallization rate and formation of the α-form crystallites in the nanocomposite fibers.[26,36,37]

The effects of the compatibilizer loading on the tensile properties and internal structure of the nanocomposite fibers containing 3.0 wt % organoclay are illustrated in Figures 10 and 11. The tensile strength slightly increased up to a compatibilizer loading of 3.0 wt % and then decreased thereafter. The elongation at break decreased up to a compatibilizer loading of 3.0 wt % and then significantly increased with increasing compatibilizer loading because the presence of the PP-*g*-MAH compatibilizer induced a more effective exfoliation of the organoclay particles. It has been reported that the extent of exfoliation of organoclay in a polymer matrix should be related to the basal spacing of the organoclay. For example, Reichert et al.[38] indirectly showed a gradual increase in the tensile properties of a nanocomposite system with respect to the organoclay *d*-spacing, which was caused by an increase in the carbon number of the alkyl substituent on the onium ion. They found a gradual increase in tensile properties as the alkyl chain length was increased from a carbon number of 4 to 8. Increasing the alkyl length from 8 to 12 carbons resulted in a significant increase in *d*-spacing and a step increase in modulus. However, the modulus leveled off beyond a carbon number of 12.

From the previous results, we inferred that countereffect of the compatibilizer played an important role in the internal structure and tensile properties of the nanocomposite fibers. The positive effect created a more effective exfoliated structure of organoclay in the PP matrix. On the contrary, a negative effect was that the nanocomposite fiber had a lower molecular weight than the pure PP fiber because the compatibilizer had a lower molecular weight than the pure PP matrix, as shown in Table I. The positive influence on the more exfoliated structure prevailed over the negative effect of the reinforcing organoclay with up to 3.0 wt % compatibilizer loading. However, above a compatibilizer loading of 3.0 wt %, the negative effect predominated over the positive effect, as shown in Figures 10 and 11. The negative effect of the compatibilizer was a result of

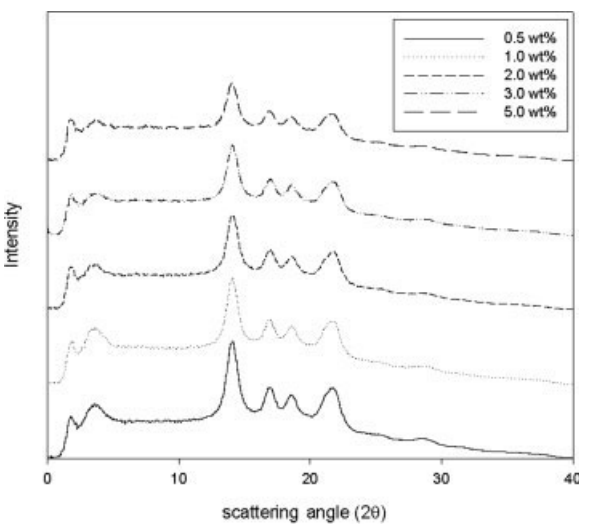

Figure 11 Effects of the PP-*g*-MAH compatibilizer loadings on the WAXD patterns of the compatibilized nanocomposite fibers with 3.0 wt % organoclay.

the low molecular weight and its influence on the decreased molecular chain orientation in the nanocomposite fibers.[39] We understood from the previous experimental results that the tensile properties of the nanocomposite fibers with organoclay and compatibilizer strongly depended on the crystal structure and the extent of exfoliation in the matrix. Because the tensile properties could be attributed to the homogeneous distribution of organoclay and to the crystalline structure of the PP/layered-silicate nanocomposite fibers, we expected that the most effective enhancement of the tensile properties was realized at the range of organoclay concentration from 1.0 to 2.0 wt % and at a compatibilizer concentration of 3.0 wt %. Although the PP-*g*-MAH compatibilizer played an important role in influencing the internal structure and tensile properties of the nanocomposite fibers in this study, a novel melt-compounding method with PP-*g*-MAH compatibilizer having a higher molecular weight or with a masterbatch process to improve the dispersion of organoclay is needed to achieve the perfect exfoliation of OLS's in the PP matrix for the production of high-performance nanocomposite fibers.

CONCLUSIONS

Compatibilized nanocomposite fibers were compared experimentally with pure PP and uncompatibilized nanocomposite fibers produced under the same spinning conditions. The morphological and rheological properties of the nanocomposite melts were investigated with SAXS, TEM, and rheometry. The nanocomposites showed nonterminal solidlike plateau behavior at a low-frequency region, higher steady shear viscosity at a low-shear rate region, and outstanding strain hardening behavior in the uniaxial elongational flow. The tensile properties of the nanocomposite fibers could be attributed to the dispersion state of the organoclay and to the varied crystallite structures. The nanocomposite fibers with organoclay and compatibilizer had lower tensile strengths and elongations at break than the pure PP fibers because they included small intercalated aggregates and well-dispersed domains. A low concentration of the organoclay resulted in dispersed domains of small sizes and uniform distributions, whereas high loadings resulted in dispersed domains of large sizes and broad size distributions. However, the PP-*g*-MAH compatibilized nanocomposite fibers showed improved tensile strength over the uncompatibilized composite fibers when compatibilizer loading was less than 3.0 wt % because the presence of the PP-*g*-MAH compatibilizer caused a more effective exfoliation of organoclay particles than its absence.

References

1. Shenoy, A. V. Rheology of Filled Polymer Systems; Kluwer Academic: London, 1999.
2. Utracki, L. A. Clay-Containing Polymeric Nanocomposites; Rapra Technology: Shropshire, England, 2004.
3. Ajayan, P. M.; Schadler, L. S.; Braun, P. V. Nanocomposite Science and Technology; Wiley-VCH: Weinheim, 2003.
4. Kawasumi, M.; Hasegawa, N.; Kato, M.; Usuki, A.; Okada, A. Macromolecules 1997, 30, 6333.
5. Sinha Ray, S.; Okamoto, M. Prog Polym Sci 2003, 28, 1539.
6. Solomon, M. J.; Almusalla, A. S. Macromolecules 2001, 34, 1864.
7. Xu, W.; Liang, G.; Zhai, H.; Tang, S.; Hang, G.; Pan, W. P. Eur Polym J 2003, 39, 1467.
8. Gupta, R. K. Polymer and Composite Rheology; Marcel Dekker: New York, 2000.
9. Carreau, P. J.; De Kee, D. C. R.; Chhabra, R. P. Rheology of Polymeric Systems; Hanser: Munich, 1997.
10. Larson, R. L. The Structure and Rheology of Complex Fluids; Oxford University Press: New York, 1999.
11. Petrie, C. J. S. Elongational Flows: Aspects of the Behavior of Model Elasticviscous Fluids; Pitman: London, 1979.
12. Salem, D. R. Structure Formation in Polymeric Fibers; Hanser: Munich, 2001.
13. Mlynarcikova, Z.; Kaempfer, D.; Thomann, R.; Mulhaupt, R.; Borsig, E.; Marcincin, A. Polym Adv Technol 2005, 6, 362.
14. Lee, S. H.; Cho, E.; Youn, J. R. J Appl Polym Sci 2007, 103, 3506.
15. Seo, Y.; Kim, J.; Kim, K. U.; Kim, Y. C. Polymer 2000, 41, 2639.
16. Lei, L.; Bellan, L. M.; Craighead, H. G.; Frey, M. W. Polymer 2006, 47, 6208.
17. Takashi, K.; Yudin, V. E.; Otaigbe, J. U.; Svetlichnyi, V. M. Polymer 2007, 48, 7130.
18. Yang, K.; Huang, Y.; Dong, J. Y. Polymer 2007, 48, 6254.
19. Wang, Y.; Chen, F. B.; Wu, K. C. J Appl Polym Sci 2004, 93, 100.
20. Kotsilkova, R. Mech Time-Depend Mater 2002, 6, 283.
21. Ren, J.; Krishnamoorti, R. Macromolecules 2003, 36, 4443.
22. Takahashi, T.; Takimoto, J.; Koyama, K. Polym Compos 1999, 20, 357.
23. Takahashi, T.; Takimoto, J.; Koyama, K. J Appl Polym Sci 1999, 72, 961.
24. Karian, H. G. Handbook of Polypropylene and Polypropylene Composites; Marcel Dekker: New York, 2003.
25. Cho, W.; Paul, D. R. Polymer 2001, 42, 1083.
26. Zheng, W.; Lu, X.; Toh, C. L.; Zheng, T. H.; He, C. J Polym Sci Part B: Polym Phys 2004, 42, 1810.
27. Joshi, M.; Viswanathan, V. J Appl Polym Sci 2006, 102, 2164.
28. Wunderlich, B.; Grebowicz, J. Adv Polym Sci 1984, 60/61, 1.
29. Svoboda, P.; Zeng, C.; Wang, H.; Lee, L. J.; Tomasko, D. L. J Appl Polym Sci 2002, 85, 1562.
30. Hasegawa, N.; Usuki, A. J Appl Polym Sci 2004, 93, 464.
31. Giza, E.; Ito, H.; Kikutani, T.; Okui, N. J Macromol Sci Phys 2000, 39, 545.
32. Ergungor, Z.; Cakmak, M.; Batur, C. Macromol Symp 2002, 185, 259.
33. Broda, J. Fibres Text East Eur 2003, 11, 115.
34. Joshi, M.; Shaw, M.; Butola, B. S. Fiber Polym 2005, 5, 59.
35. Pavlikova, S.; Thomann, R.; Reichert, P.; Mulhaupt, R.; Marcincin, A.; Borsig, E. J Appl Polym Sci 2003, 89, 604.
36. Zhang, X.; Yang, M.; Zhao, Y.; Zhang, S.; Dong, X.; Liu X.; Wang, D.; Xu, D. J Appl Polym Sci 2004, 92, 552.
37. Jin, Y.; Rogunova, M.; Hiltner, A.; Baer, E.; Nowacki, R.; Galeski, A.; Piorkowska, E. J Polym Sci Part B: Polym Phys 2004, 42, 3380.
38. Reichert, P.; Nitz, H.; Klinke, S.; Brandsch, R.; Thomann, R.; Mulhaupt, R. Macromol Mater Eng 2000, 275, 8.
39. Vlasveld, D. P. N.; Bersee, H. E. N.;Picken S. J. Polymer 2005, 46, 10269.